

Herbig-Haro flows in L1641N ^{★,★★}

M. Gålfalk¹ and G. Olofsson¹

Stockholm Observatory, Sweden

Received 01 December 2006 / Accepted 06 February 2007

ABSTRACT

Aims. To study the Herbig-Haro (HH) flows in L1641N, an active star formation region in the southern part of the Orion GMC and one of the most densely populated regions of HH objects in the entire sky. By mapping the velocities of these HH objects, combined with mid-IR observations of the young stars, the major flows in the region and the corresponding outflow sources can be revealed.

Methods. We have used the 2.56 m Nordic Optical Telescope (NOT) to observe two deep fields in L1641N, selected on the basis of previous shock studies, using the 2.12 μm transition of H₂ (and a K_S filter to sample the continuum) for a total exposure time of 4.6 hours (72 min K_S) in the overlapping region. The resulting high-resolution mosaic (0.23" pixel size, 0.75" seeing) shows numerous new shocks and resolves many known shocks into multiple components. Using previous observations taken 9 years earlier we calculate a proper motion map and combine this with Spitzer 24 μm observations of the embedded young stars.

Results. The combined H₂ mosaic shows many new shocks and faint structures in the HH flows. From the proper motion map we find that most HH objects belong to two major bi-polar HH flows, the large-scale roughly North-South oriented flow from central L1641N and a previously unseen HH flow in eastern L1641N. Combining the tangential velocity map with the mid-IR Spitzer images, two very likely outflow sources are found. The outflow source of the eastern flow, L1641N-172, is found to be the currently brightest mid-IR source in L1641N and seem to have brightened considerably during the past 20 years. We make the first detection of this source in the near-IR (K_S) and also find a near-IR reflection nebula pointing at the source, probably the illuminated walls of a cone-shaped cavity cleared out by the eastern lobe of the outflow. Extending a line from the eastern outflow source along the proper motion vector we find that HH 301 and HH 302 (almost 1 pc away) belong to this new HH flow.

Key words. ISM: jets and outflows – infrared: ISM: lines and bands – stars: formation – ISM: individual objects: L1641N

1. Introduction

Very young stars are often associated with molecular bi-polar outflows and jets/shocks that emit both atomic and molecular lines. At early stages, the outflow and in-fall are believed to occur simultaneously as the stellar core is formed. These outflows are a good tracer of ongoing star formation, but it is often difficult to exactly localise the central source which is usually heavily obscured. While single-dish millimetre observations can reveal molecular outflows from deeply embedded stars at very early stages, they suffer from poor spatial resolution and therefore from source confusion in crowded regions. Optical surveys (most often H α and [SII] 6707,6717 nb imaging) instead often suffer from too high extinction and works best for the blue-shifted lobe of Herbig-Haro (HH) flows with high inclinations. The shock-heated gas often give rise to H₂ emission, and by observing e.g. the 2.12 μm line, the cloud extinction is less of a problem. However, the faintness of the emission means that deep images are essential to study these flows in detail.

Send offprint requests to:

M. Gålfalk, e-mail: magnusg@astro.su.se

* Based on observations made with the Nordic Optical Telescope, operated on the island of La Palma jointly by Denmark, Finland, Iceland, Norway, and Sweden, in the Spanish Observatorio del Roque de los Muchachos of the Instituto de Astrofísica de Canarias.

** This work is based in part on observations made with the Spitzer Space Telescope, which is operated by the Jet Propulsion Laboratory, California Institute of Technology under a contract with NASA.

Lynds 1641 (L1641) is a dark molecular cloud, located in the southern part of our nearest giant molecular cloud Orion A (d~450pc). It hosts sites of active star formation (Strom et al. 1989), and attention was drawn to the northern part of the cloud, simply called L1641N, in the mid 80s with the discovery of a molecular outflow (Fukui et al. 1986) at the position of the mid-IR bright source IRAS 05338-0624. Fukui et al. (1988) found well-separated lobes to the North (blue-shifted) and South (red-shifted) of the IRAS source using CO observations of higher resolution. Further observations have been made through molecular line studies (e.g. Chen et al. 1996, Sakamoto et al. 1997 and Stanke et al. 2006/2007), Optical and near-IR surveys (e.g. Strom et al. 1989, Hodapp & Deane 1993, Chen et al. 1993) and in the mid-IR (Gålfalk et al. 2007).

L1641N is presently the most active site of low-mass star formation in the L1641 molecular cloud and has one of the very highest concentrations of HH objects known anywhere in the sky (Reipurth et al. 1998). HH shocks in these flows have been observed in both the near-IR 2.12 μm line of H₂ (Davis et al. 1995, Stanke et al. 1998) and in the optical lines H α and the [SII] doublet (Reipurth et al. 1998, Mader et al. 1999). In a forthcoming paper (Gålfalk et al. 2007) we study the young stellar population in L1641N using ISO, Spitzer, ground based photometry and spectroscopy. In this contribution we instead focus on the HH flows using our recent 2.12 μm H₂ observations (which are the deepest and highest resolution observations yet of the HH flows in L1641N). We have mapped the proper motions of shock heated H₂ and related these flows to embedded young stars seen

in the mid-IR. Throughout the paper we use the notation *shocks* as short for *shock heated regions*.

2. Observations and reductions

2.1. Narrow band $2.12\mu\text{m}$ and K_S band imaging

We have made deep observations of the shocks and jets in L1641N using the $2.12\mu\text{m}$ S(1) line of H_2 . Since this line is close to the centre of our K_S filter ($2.14\mu\text{m}$) we used this broad band filter to sample the continuum. This is of course a much quicker (although probably not as accurate) method than using equal amounts of exposure time with a continuum nb filter to one side of the line. It also provides a well defined band for point source photometry of the outflow sources. The observations were made on two photometric nights at the Nordic Optical Telescope (NOT) on Dec 13-15 2005 with an average seeing of $0.75''$ (0.60 – $0.85''$) using NOTCam with the newly installed science-grade array. NOTCam is an HAWAII 1024x1024x $18.5\mu\text{m}$ pixels HgCdTe array with a field-of-view of $4.0'' \times 4.0''$. Two positions were selected on the basis of including as many interesting jets and Herbig-Haro objects as possible in order to relate these to embedded outflow sources. Both regions include central L1641N which thus has an increased total exposure time. The first deep field is centred on a position ($05^{\text{h}}36^{\text{m}}24.07^{\text{s}}$, $-06^{\circ}23'01.9''$, Epoch 2000) close to the brightest mid-IR source in L1641N (L1641N-172, see Gålfalk et al. 2007). The second deep field, centred on ($05^{\text{h}}36^{\text{m}}13.94^{\text{s}}$, $-06^{\circ}20'52.5''$, Epoch 2000) images the NW part of L1641N but also overlaps the first mosaic as the central part of L1641N is included in both fields.

All NOTCam observations are differential, meaning that the bias frame and dark current are removed automatically through on-off calculations. A median sky is subtracted from the target (with equal exposure time) and in these observations, where we do not have any really extended objects, we use small-step dithering between each exposure and calculate a median sky from the on frames themselves. The flat-fielding is also differential (sky-flats observed with some time delay and subtracted). Besides the usual reduction steps of near-IR imaging, we have used our NOTCam model (Gålfalk 2005) to correct for image distortion and some other in-house routines (written in IDL) to find and remove bad pixels, shift-add images and to remove all the dark stripes that results from lowered sensitivity after a bright source has been read out of the detector array - this could go unnoticed for normal imaging but when a deep field is made with a lot of overlaps a complicated pattern may result (especially after distortion correction) that has to be corrected for in order to be able to keep a high contrast in the mosaics.

The individual exposure times are 14.4 s and 60 s for the K_S band and $2.12\mu\text{m}$ nb filter respectively. In the final mosaics, including both nights, total exposure times are 2880 s and 10500 s for K_S and $2.12\mu\text{m}$ respectively at position 1 and 1440 s and 6000 s respectively at position 2. In the central region of L1641N, where both images overlap we thus get total exposure times of 4320 s and 16500 s respectively in the two filters. We reach a 3σ H_2 surface brightness limit of $4.8 \times 10^{-17} \text{ erg s}^{-1} \text{ cm}^{-2} \text{ arcsec}^{-2}$ and detect point-sources down to $K_S \sim 19.5$ mag.

2.2. Additional ground based observations

2.2.1. First epoch $2.12\mu\text{m}$ H_2 imaging

In order to map the proper motions of the jets and HH objects we needed a previous epoch of $2.12\mu\text{m}$ observations, with a large enough time span to show the proper motions with reasonable accuracy, but at the same time with high enough quality to show as many of our recently observed H_2 objects as possible given that the new epoch is a deep field. We would like to thank Stanke et al. for providing us with the much needed first epoch observations, that were carried out on Dec 26 1996 using the Omega-Prime camera on the Calar Alto 3.5 m telescope. For details of these observations we refer to Stanke et al. (1998). Using this mosaic we thus get a time span of almost exactly 9 years, and since the same type of detector array was used for both epochs the quality is comparable, except for our much longer total exposure time (obtainable by only imaging L1641N).

2.2.2. Optical imaging (I band)

Optical observations are very useful in order to clearly show reflection nebulosity on our side of the cloud. We have made I band observations on 04 December 2003 using the ALFOSC (Andalucia Faint Object Spectrograph and Camera) on the Nordic Optical Telescope (NOT). This instrument has a 2048×2048 CCD and at a PFOV of $0.188''/\text{pixel}$ it has a FOV of about $6.4'' \times 6.4''$. A 5×5 mosaic was made with individual exposure times of 60 s using step sizes of $23''$ and $30''$ in RA and Dec respectively, leading to a total exposure time of 25 minutes throughout most of the mosaic.

2.3. Spitzer Space Telescope

Spitzer carries a 85 centimetre cryogenic telescope and three science instruments, one of these is the Multi-band Imaging Photometer for Spitzer (MIPS) that contains three separate detector arrays, making simultaneous observations possible at 24, 70, and $160\mu\text{m}$. Another instrument is the Infrared Array Camera (IRAC), providing simultaneous $5.2'' \times 5.2''$ images in four channels, centred at 3.6, 4.5, 5.8 and $8.0\mu\text{m}$. Each channel is equipped with a 256×256 pixel detector array with a pixel size of about $1.2'' \times 1.2''$.

The Spitzer data used in this paper was obtained from the Spitzer Science Archive using the Leopard software, and all data had been reduced to the Post-Basic Calibrated Data (pbcd) level. We used MIPS data from the program “A MIPS Survey of the Orion L1641 AND L1630 Molecular Cloud” (Prog.ID 47) and IRAC data from the program “An IRAC Survey of the L1630 and L1641 (Orion) Molecular Clouds” (Prog.ID 43), both with G. Fazio as the P.I. We used the $24\mu\text{m}$ observations of the MIPS program. These observations cover a much larger region than we need, however, L1641N is covered in the giant mosaic. The $24\mu\text{m}$ camera has a resolution of 128×128 pixels and a pixel size of $2.55''$. In order to plot Spitzer contours on our ground-based observations, although very different resolutions, we matched all stars seen in the Spitzer $24\mu\text{m}$ mosaic with our K_S band observations and corrected for differences in FOV, distortion and image rotation.

Even though the IRAC data had been reduced to the pbcd level there was still a lot of artefacts, background variations and varying orientation in the mosaics. For this reason we used our own in-house routines to reduce the data further (this was possible since we had eight overlapping mosaics to merge in

each channel). These additional reductions include cosmic ray removal, de-striping (most likely pick-up noise), removing the large background variations between regions in the same mosaic and between mosaics, marking bad pixels not to be used further, removing ghost-effects from bright sources, de-rotation, shifting, adding and making a composite colour image. This required some work, but since we only needed to reduce the L1641N region (and these mosaics are huge) we could concentrate on just that part - which because of all mosaics having different rotations meant first finding L1641N in each one and cropping them to manageable sizes.

3. Proper motion calculations and accuracy

In order to warp the first epoch images to match the second epoch we start by measuring the positions of all stars visible in both observations by fitting a two-dimensional elliptical Gaussian equation to each star, including rotation. Writing the equation as

$$F(x, y) = A_0 + A_1 \cdot e^{-U/2} \quad (1)$$

and using the elliptical function

$$U = (x'/a)^2 + (y'/b)^2 \quad (2)$$

we can include clockwise rotation α with the centre at (x_c, y_c) and write x' and y' as

$$x' = (x - x_c) \cdot \cos \alpha - (y - y_c) \cdot \sin \alpha \quad (3)$$

$$y' = (x - x_c) \cdot \sin \alpha + (y - y_c) \cdot \cos \alpha \quad (4)$$

A gradient-expansion algorithm is used to compute a non-linear least squares fit to Eq.1 for the parameters α, a, b, A_0, A_1 and more importantly the centre of the PSF (x_c, y_c) . This method has proven to give very accurate sub-pixel positions of stars, accounting for both seeing variations and elliptically shaped stars due to the optics in the telescope system (image distortion).

Assuming that the stars, on average, have negligible proper motions and denoting image coordinates in the first epoch (x_0, y_0) and second epoch (x_1, y_1) we then use a least squares estimate to fit the following polynomial transformation functions:

$$x_1 = \sum_{i=0}^2 \sum_{j=0}^2 A_{i,j} \cdot x_0^j \cdot y_0^i \quad (5)$$

$$y_1 = \sum_{i=0}^2 \sum_{j=0}^2 B_{i,j} \cdot x_0^j \cdot y_0^i \quad (6)$$

Even though differences in distortion, field of view and possible slight image rotation between the two epochs have been corrected for using this method there are several sources of uncertainty related to the geometry and physics of both the HH objects and the reference stars themselves. Some fast moving stars can have proper motions comparable to that of slow moving shocks and thus increase the uncertainty of the image matching in parts of the image with few stars. The shocks themselves change shape with time, some much more than others and for some objects the proper motion varies a lot within the shock itself. Another complicated situation is encountered for HH objects that are extended along the direction of motion that also lack bright knots that could have been used for easy measurements.

Table 2. Selected L1641N sources^a.

No.	RA (2000)	Dec (2000)	K_s (mag)	Comment
61	05:36:10.44	-06:20:01.5	10.85 ± 0.01	
110	05:36:17.86	-06:22:28.6	15.28 ± 0.08	
114	05:36:18.48	-06:20:38.7	11.00 ± 0.01	V832 Ori
115	05:36:18.49	-06:22:13.6	...	
116	05:36:18.81	-06:22:10.6	...	
124	05:36:19.50	-06:22:12.1	16.40 ± 0.15	Central flow
145	05:36:21.87	-06:23:30.1	10.71 ± 0.02	
172	05:36:24.61	-06:22:41.7	15.67 ± 0.04	Eastern flow

^a All data and source numbers in this Table are from our forthcoming paper on the IMF in L1641N. The full catalogue contains 216 sources.

Using the two matched epoch images each proper motion is calculated by sub-pixel shifting the second epoch image so that a shock (or part of a shock in cases where the proper motion varies within the shock) overlap in both images. This is done manually in steps of 0.1 pixels along both axes while blinking both images at different frame rates as well as simultaneously displaying them in different colour channels in another window (first epoch in red colours and second epoch in green). When a shock overlaps itself it appears to be stationary and no colour separations are seen, the positional shifts are estimated to an accuracy of ± 0.2 pixels in both directions. Another way to do this would be by using cross-correlation, but this would however not work for shocks close to stars. Another advantage with the manual method is that we can measure proper motions for shocks that have varying velocities along the shock or choose a point-like or sharp features that is especially easy to follow.

4. Results and discussion

Our two $2.12\mu\text{m}$ H_2 deep fields are presented as colour composite images in Figures 1 and 2 with the $2.12\mu\text{m}$ observations as yellow and the continuum (K_s band) as blue. Using an appropriate intensity scaling between the line and continuum images and by adding a constant to one of the images to make the sky background equal is an efficient way to separate H_2 emission from continuum features without the need to look back and forth at the line and continuum images. We have continued the H_2 shock naming scheme started by Stanke et al. (1998) and added newly discovered objects using letters (e.g. 14 R-V) and objects resolved into several components or newly discovered components by sub-group numbers and letters (e.g. 14 F is separated into 14 F₁ and F₂, 14 E₁ is seen as the three components E_{1A}-E_{1C}). In Fig.1 most shocks belong to group 14 and only the sub-groups (A-V) are shown for clarity, but for the H_2 features in groups 16 and 20 the group number is shown for each object in order to avoid confusion. Group 8, seen in Fig.2 is part of the same flow as the group 14 shocks. In the following, when we refer to the embedded stars themselves by a number (e.g. L1641N-172, or No. 172 for short) we use the source numbering found in our forthcoming paper on the IMF in L1641N (Gålfalk et al. 2007). Our full catalogue contains a total of 216 sources, whereas Table 2 only lists the small selection of these sources that are discussed in this paper.

The results of our proper motion measurements throughout L1641N are presented in Table 1. As shown in the Table the tangential velocities (assuming a distance of 450 pc) are in the

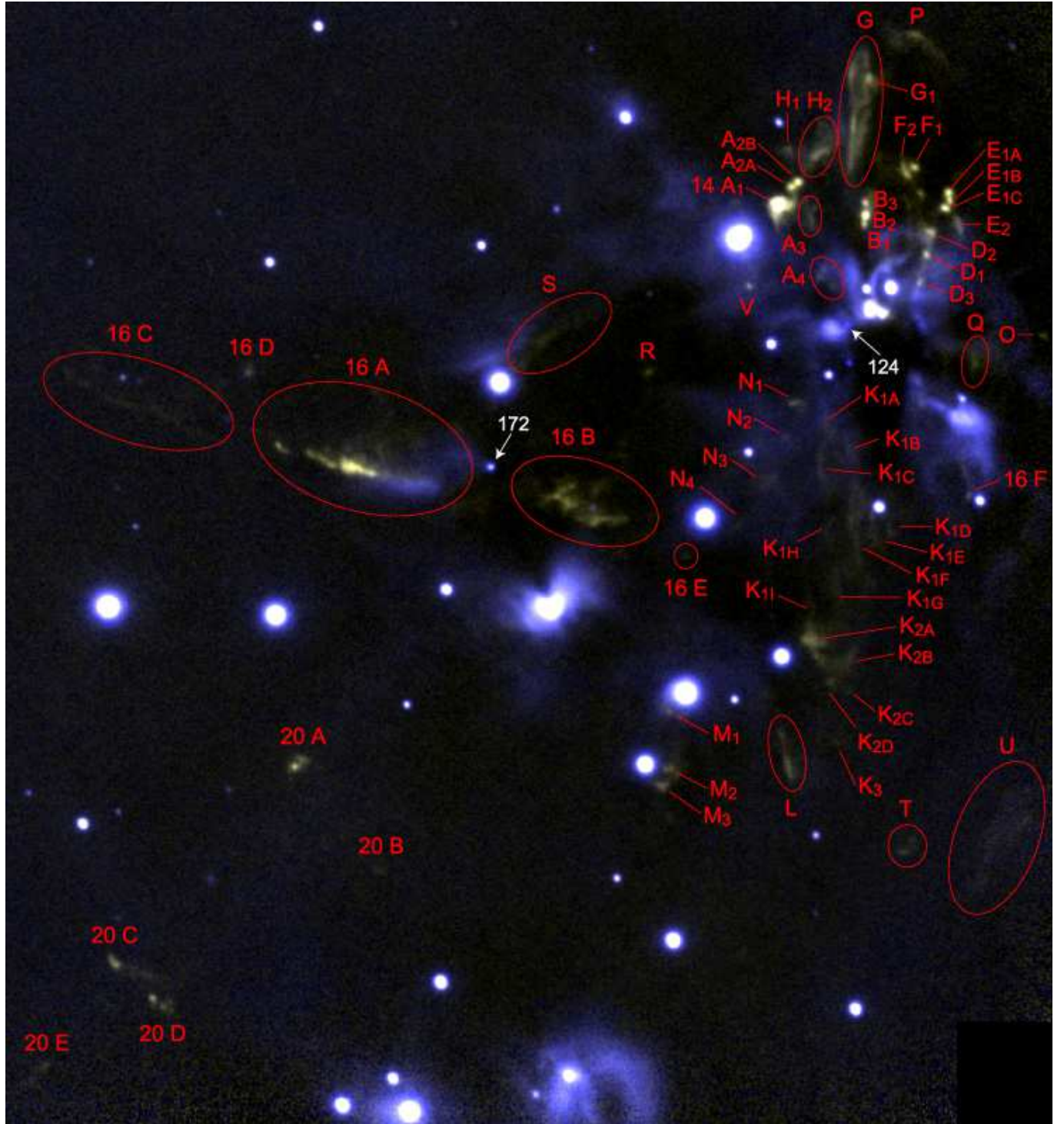


Fig. 1. Deep K_s (blue) and $2.12\mu\text{m}$ H_2 (yellow) colour composite of the central and South-East region of L1641N including names of all visible H_2 features. Most of the features in this Figure belong to group 14, for clarity the prefix for these objects have been dropped. Features belonging to the two other groups (16 and 20) are clearly marked with their group name. The field shown has a size of 3.64×3.90 and is centred on $05^h36^m24.07^s$, $-06^{\circ}23'01.9''$ (epoch 2000) - close to the eastern outflow source. The two arrows indicate the suggested outflow sources (L1641N-124 and 172).

range $30\text{--}230\text{ km s}^{-1}$. The lower value also roughly represent the detection limit. Since the radial velocities of these H_2 features are unknown the measurements are lower limits of the real three dimensional velocities, yet some of the proper motions suggest velocities in excess of 200 km s^{-1} , much higher than the dissociation speed limit of H_2 in molecular shocks of ~ 25

and $\sim 50\text{ km s}^{-1}$ for J- and C-type shocks, respectively (Smith 1994). This may at first seem like a contradiction, given that all the proper motions were measured and thus clearly seen in H_2 emission (suggesting low shock velocities). Proper motions are however not necessarily a direct measurement of the shock speed for several reasons. Proper motions measure the

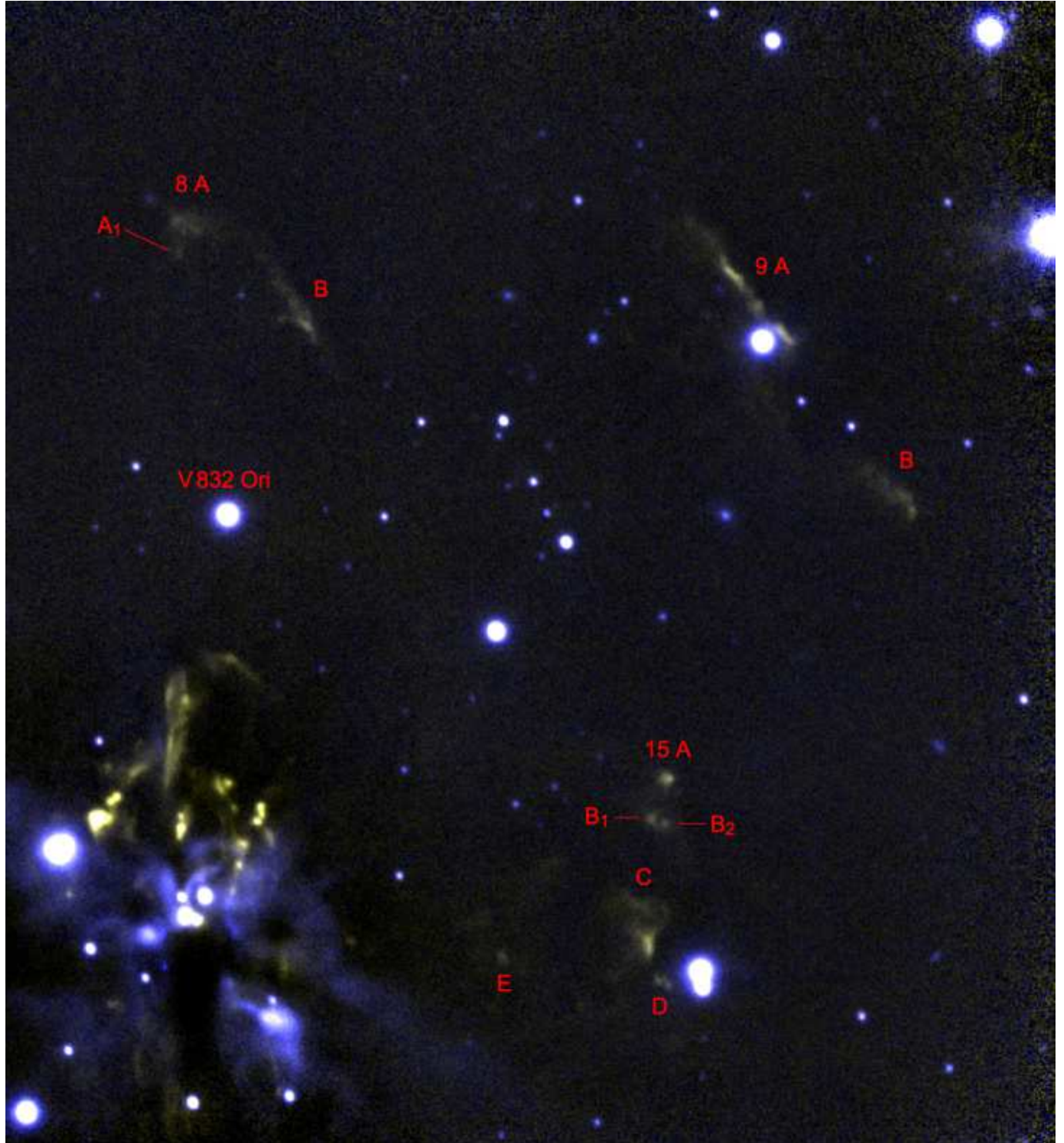


Fig. 2. Deep K_S (blue) and $2.12\mu\text{m}$ H_2 (yellow) colour composite of the central and North-West region of L1641N including names of all visible H_2 features. The field shown has a size of 3.84×4.18 and is centred on $05^{\text{h}}36^{\text{m}}13.94^{\text{s}}$, $-06^{\circ}20'52.5''$ (Epoch 2000).

pattern speed of these features, but for example in the case of flow variability (Raga 1993) the pre-shock gas could also be non-stationary resulting in internal working surfaces in the flow, bounded by a leading and a trailing reverse shock, possibly with only marginally faster material moving into somewhat slower gas and therefore much lower shock velocities than suggested directly from the pattern speed. Also, since the shock speed is locally determined by the velocity perpendicular to the shock surface, in a bow shock there is a range of shock velocities in-

volved from the fast shock at the apex to the much slower shocks in the wings. This then means that even if a bow shock is much faster than the dissociation speed at its apex, there could still be bright H_2 emission coming from the wings (see e.g. the bow shock models in Smith et al. 2003). Several other $2.12\mu\text{m}$ H_2 proper motion surveys of star-formation regions have also resulted in tangential velocities much higher than the H_2 dissociation speed limit for both J- and C-shocks (Coppin et al. 1998; Micono et al. 1998; Lee et al. 2000).

Table 1. Proper motion results. Column 1, the shock designations, are given in Figures 1 and 2. Columns 2–4 give the angular distance each shock has moved between the two epochs (almost 9 years apart). Columns 5–7 are the proper motions and finally Columns 8–9 the (tangential) velocities and positional angles. Uncertainties are given at the bottom of the table (except for the PA where this is given in each row).

Shock	Δ_α ($''$)	Δ_δ ($''$)	Δ_{tot} ($''$)	μ_α (mas/yr)	μ_δ (mas/yr)	μ_{tot} (mas/yr)	vel (km/s)	PA ^a (deg)	Comment
(1)	(2)	(3)	(4)	(5)	(6)	(7)	(8)	(9)	(10)
8 A	-0.19	+0.61	0.64	-21	68	71	152	343 \pm 6	
B	-0.07	+0.31	0.31	-8	+34	35	75	347 \pm 12	
14 G	+0.14	+0.94	0.95	+16	+105	106	227	9 \pm 4	North (fastest) part
G ₁	+0.00	+0.19	0.19	0	+21	21	45	0 \pm 19	
H ₁	+0.07	+0.24	0.25	+8	+26	27	58	17 \pm 14	
K _{1A}	+0.00	-0.14	0.14	0	-16	16	34	180 \pm 27	
K _{1C}	+0.00	-0.16	0.16	0	-18	18	39	180 \pm 22	
K _{1F}	+0.24	-0.42	0.48	+26	-47	54	115	151 \pm 8	
K _{2A}	+0.12	-0.47	0.49	+13	-53	54	116	166 \pm 8	
K _{2B}	+0.09	-0.89	0.90	+11	-100	100	214	174 \pm 4	
K _{2D}	+0.12	-0.89	0.90	+13	-100	101	215	173 \pm 4	
L	+0.05	-0.52	0.52	+5	-58	58	124	175 \pm 7	
M ₂	+0.14	-0.26	0.30	+16	-29	33	70	151 \pm 13	
M ₃	+0.14	-0.26	0.30	+16	-29	33	70	151 \pm 13	
P	+0.07	+0.68	0.69	+8	+76	77	163	6 \pm 5	
R	+0.59	-0.26	0.64	+66	-29	72	153	114 \pm 6	
V	-0.47	-0.42	0.63	-53	-47	71	151	228 \pm 6	
16 A	+0.31	+0.07	0.31	+34	+8	35	75	77 \pm 11	
B	-0.40	+0.00	0.40	-45	0	45	95	270 \pm 8	
D	+0.35	-0.28	0.45	+39	-32	50	108	129 \pm 9	
	\pm 0.05	\pm 0.05	\pm 0.07	\pm 6	\pm 6	\pm 8	\pm 16		

^a Position Angle: North 0°, East 90°, South =180°, West 270°.

In Fig.3 as an overview we present all proper motions drawn on a colour composite mosaic (K_S , 2.12 μm H₂ and I) of the full surveyed region. Spitzer 24 μm flux contours are also overplotted since cold, deeply embedded young stars are bright at these wavelengths. The projected velocity vectors are drawn using two colours, white arrows relate to H₂ features of the major flows while red arrows are used for features with unknown origins. The general impression from all shocks with measurable proper motions, in combination with the Spitzer 24 μm contours, is that most shocks are either part of the bi-polar large scale North-South moving flow emanating from central L1641N or a previously undetected roughly East-West bi-polar HH flow originating at the other strong 24 μm source, also clearly seen in our K band image. In addition to this, there are a large amount of H₂ features where no motion is detected at our present resolution (pixel size of 0.40'' and 0.23'' for the epochs) and time span (9 years) meaning that they are most likely shocks with small projected velocities (slower than about 30 km s⁻¹). These features have been marked with an x in Fig.3. While the morphology of features like 14 D₁–D₃ and E₁ (knots lying almost exactly along a line through the very central of L1641N) suggest a HH flow nature, other features (e.g. groups 9, 15 and 20) lack this morphology and could possibly be PDR-style fluorescently-excited layers and filaments in the surrounding cloud.

4.1. The eastern flow

Spitzer observations of the eastern bi-polar flow using IRAC (3.6, 4.5 and 8.0 μm) are shown in Fig.4. The field of view extends beyond the eastern border of our 2.12 μm mosaic. Following the proper motion of shocked H₂ in jet 16 A close to

the mid-IR bright source L1641N-172 (as shown by the arrow) leads to a group of objects that also have morphologies consistent with bow shocks. This is in fact HH 301 and as can be seen in the wide-field H₂ mosaic of Stanke et al. (1998), continuing along this line leads to HH 302. It has been seen in several other Spitzer surveys (e.g. Noriega-Crespo et al. 2004 and Harvey et al. 2006) that IRAC channel 2 (4.5 μm) is very efficient in detecting Herbig-Haro objects. The reason for this is partly that the spectral response function is highest in this channel, but there are at least two more contributing factors. Between approximately 4–5 μm there are many vibrational and rotational H₂ emission lines, these have been modeled by Smith & Rosen (2005) for all IRAC bands using three-dimensional hydrodynamic simulations of molecular jets. The strongest integrated H₂ emission is predicted to arise from band 2 because of rotational transitions. For the typical conditions of low-mass outflows, pure-rotational transitions like S(11)–S(4) (4.18–8.02 μm) can actually be much brighter than the standard 2.12 μm H₂ line (Kaufman & Neufeld 1996). Channel 2 is also the most “PAH-free” band of IRAC, greatly enhancing its usefulness as a HH tracer, as opposed to the 5.8 and 8.0 μm channels (see Fig.4) which include bright, diffuse emission from polycyclic aromatic hydrocarbons (PAHs), hiding the shock-excited H₂ features of the HH flows.

Both HH 301 and HH 302 are therefore very likely part of the eastern HH-flow, originating from L1641N-172, which we confirm as the outflow source using proper motions, near-IR 2.12 μm H₂ morphology and mid-IR photometry at 3.6, 4.5, 5.8, 8.0 and 24 μm . HH 302 is located \sim 6.3' away from L1641N-172 (corresponding to 0.83 pc at the assumed distance of 450 pc) suggesting that this is a large-scale flow. In the opposite direction in the same wide-field mosaic there is another HH object (called 19

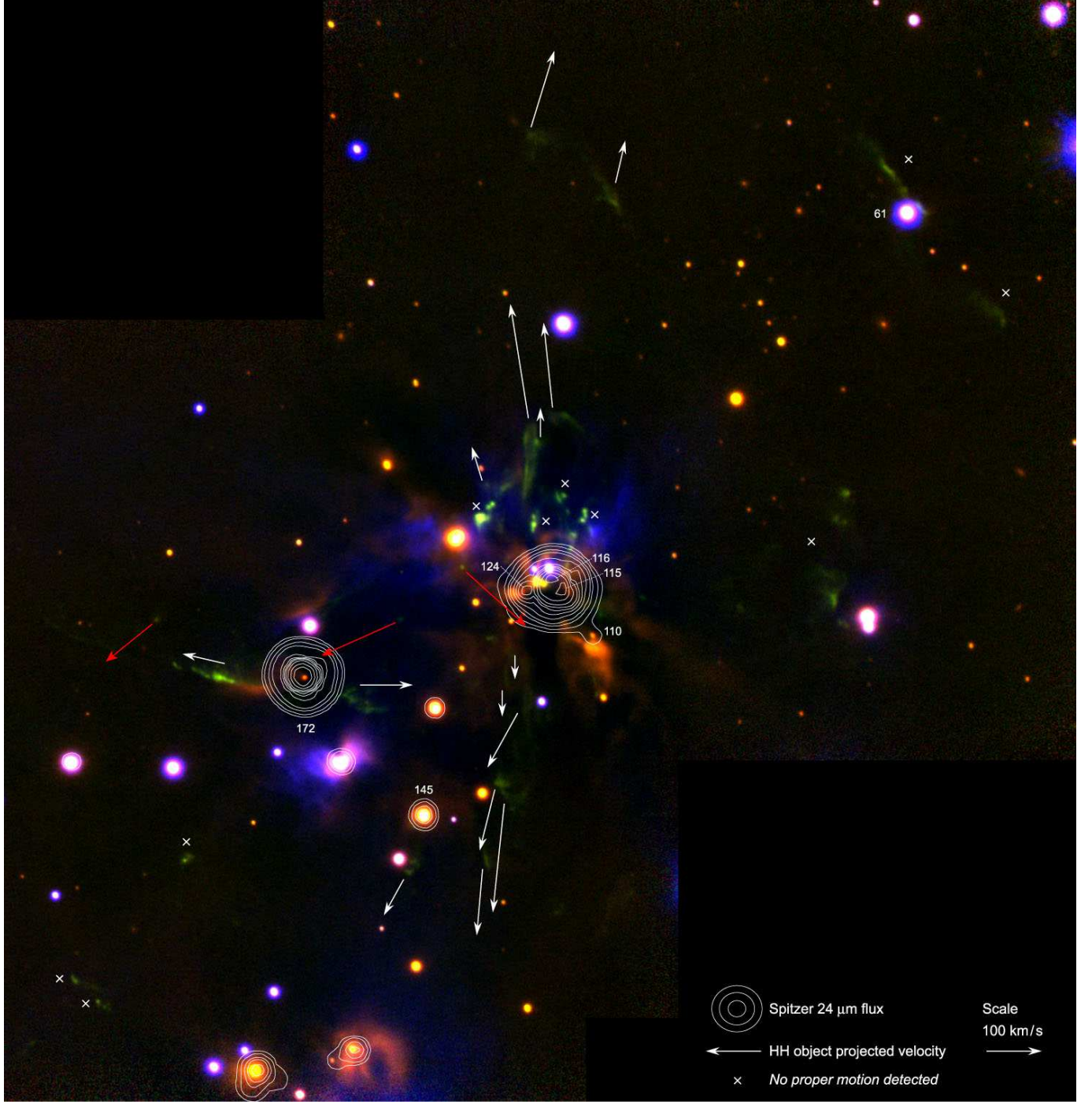


Fig. 3. Flow chart of Herbig-Haro objects. Proper motions are indicated by arrows overplotted on a colour composite of our K_S (red), $2.12\mu\text{m}$ H_2 (green) and I (blue) mosaics. White arrows indicate HH objects that are suggested by their proper motions to be part of either the major North-South oriented HH flow emanating from central L1641N or part of the proposed new HH flow. Red arrows are used for single HH objects with uncertain origin. Bright HH objects for which we detect no movement are marked with an x. Spitzer $24\mu\text{m}$ contours are also overplotted, revealing the most embedded and young stars, responsible for the jets and shocks. Numbers refer to deeply embedded sources as given in Gålfalk et al. (2007) and Table 2. The field of view of this mosaic is roughly $6.1' \times 6.3'$.

in Stanke et al. 1998) that could also be part of the flow, although proper motions are required to confirm this.

Note that the proper motion vector of the H_2 feature in the counter-flow 16B (West of the outflow source) only refers to its fast moving northern part. There seems to be very different velocities involved across feature 16B and the proper motion vector may just represent the fastest moving part in a probable

cone-like outflow with a similar opening angle as on the other side of the outflow source.

As can be seen in Fig.3 the position of the outflow source, L1641N-172, coincides very well in the K_S and $24\mu\text{m}$ observations. Looking at the two epochs we use for proper motion calculations this source has brightened considerably in the last 9 years (and comparing IRAS and ISO observations it seems

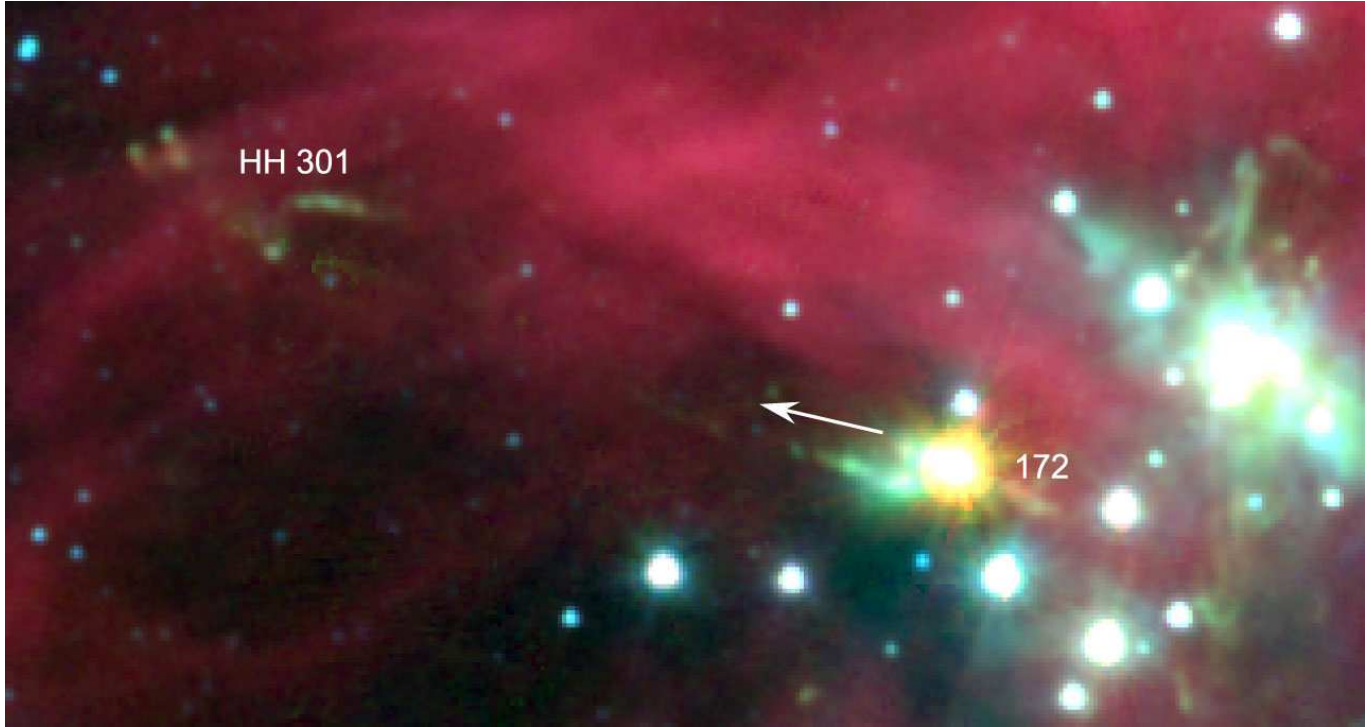


Fig. 4. Spitzer colour mosaic of the eastern flow using IRAC channels $3.6\mu\text{m}$ (blue), $4.5\mu\text{m}$ (green) and $8.0\mu\text{m}$ (red). L1641N-172 is very bright (even saturated) in the $4.5\mu\text{m}$ and $8.0\mu\text{m}$ images. Shocked H_2 is clearly seen in the $4.5\mu\text{m}$ band close to L1641N-172 at the same position as in our $2.12\mu\text{m}$ observations. Following the direction of proper motion (shown by the arrow) leads to a group of H_2 shocks (HH 301) outside of our $2.12\mu\text{m}$ mosaic (see Fig.1). The field of view is 6.1×3.3 . North is up and East is left in all Figures.

to have brightened a lot over the decade before that as well). Since this source is not detected in the first epoch K_S mosaic (limiting magnitude $K_S \sim 17$) we can however only give a lower limit of 1.5 mag. for the increased brightness between the two epochs. L1641N-172 is extremely bright in the mid-IR and saturates Spitzer at 4.5 , 5.8 and $8.0\mu\text{m}$. In our new K_S images there is also clearly a cone-shaped reflection nebula pointing at the outflow source, which is apparently lit up by the now much brighter source. The shape of the nebula suggests that it could be the illuminated walls of a cone-shaped cavity cleared out by this previously undetected flow.

Both this new bi-polar HH flow and its suggested outflow source (L1641N-172) are supported by recent CO observations (Stanke et al. 2006/2007, to be published) which reveal a bi-polar CO outflow centred on this source, with a blue-shifted lobe roughly to the East (B-E) and a red-shifted lobe to the West (R-E), in agreement with our proper motions.

HH 298 is an East-West chain of three HH knots about $70''$ long, originally reported in Reipurth et al. 1998. We note that there seems to be some general confusion about this object in several publications. Reipurth et al. states knot A as the brightest knot in $\text{H}\alpha$ and [SII], which is the westernmost knot as is also marked in their Fig.5, but gives its coordinates as the easternmost knot (which is knot C in their text). In Mader et al. (1999) HH 298 A is given (in their Fig.9) as a different source that is not close to either knot HH 298 A, B or C but instead close to our discovered outflow source of the eastern HH flow, L1641N-172. They also suggest N23 of Chen et al. (1993) as the outflow source for HH 301 and HH 302. However, we do not detect any point source at that position in our deep field (it is probably a bright H_2 knot in the 16 A jet that Chen et al. detected in the K band as N23). Only the westernmost (and optically brightest)

knot of HH 298 has an IR counterpart. It corresponds to shocks E_{1A} – E_{1C} which are the three outermost knots in a well-defined chain of knots towards the NNW from central L1641N. Thus, the three knots of HH 298 (lying on a E-W line) cannot be part of the same flow, as seen from geometry.

4.2. The central North-South flow

Comparing the velocities in this flow there are many knots with no measurable proper motions near the central source, while further out features with large proper motions are seen. This is roughly consistent with a bubble flow, though obviously orientation will play a major role. Using two bright, well-defined bow shocks (14 K_{2B} and 14 P) with accurate proper motions, we find that very similar ages are implied (730 and 780 years respectively). This suggests that they were probably ejected in the same event. Looking at the bow shock 8 A further to the north (with an implied age of 2200 years) this seems to be the leading shock front of an earlier event. Shocks from older outbursts than that have probably moved out of our observed region. Following the mean velocity vector South in a wide field mosaic (Fig.1 of Stanke et al. 1998) we find groups of HH objects (23 A, B, D, E, F, G) far away from the source. Similarly, following the velocity vector of the northern flow we find two groups (4 A and B) of shocks at about the same distance from the outflow source as 23 F but on the other side. This is thus a very large-scale outflow extending several parsecs as seen in the IR. There is a bright star, V832 Ori (L1641N-114), in the north lobe of the central flow (see Fig.2). In our survey of young stars in L1641N (Gålfalk et al. 2007) optical spectra show this to be a young star with $T_{\text{eff}} = 3800\text{ K}$ and an IR excess at $8.0\mu\text{m}$ (as seen in our Spitzer photo-

tometry). This star does however not show any evidence in our $2.12\mu\text{m}$ images of being physically related to the HH flow in any way.

We make the first detection of a previously proposed central outflow source, L1641N-124, in the near-IR ($K_S = 16.40 \pm 0.15$). This source is very bright in the mid IR, it saturates Spitzer at $8.0\mu\text{m}$ and has a high flux at $24\mu\text{m}$. The proper motions in the flow suggest this as the most likely outflow source to the giant, North-South flow. There is a bright reflection nebula next (to the East) to this source. Chen et al. (1993) have observed this source (called N15 in their paper) in the M band, however, their H and K source is in fact the nearby reflection nebula since it looks extended and is displaced to the East of the outflow source.

The central region is very crowded with H_2 shocks, especially to the north, complicating the situation of a single outflow source. While L1641N-124 is the most likely major outflow source (most easily seen from the proper motions in the southern part) there are probably also outflows from L1641N-115, 116 and 110. An example of this is the very collimated chain of H_2 knots pointing out from a position close to L1641N-115 and 116 to the NNW (objects 14D₁–D₃ and E_{1A}–E_{1C}). Since no proper motion is detected in this chain of shocks it is either slow or has a different inclination (more radial than tangential) than the major flow which in that case suggests a different outflow source that could very well be No. 115 or 116. It is probably the blue-shifted jet that we see in the NNW flow since no counter-jet is seen to the SSE.

We cannot rule out (using proper motions or the $24\mu\text{m}$ flux) the possibility that L1641N-115 or 116 contribute to the giant, North-South flow. One reason for this is that even though the northern jet-like feature (14G) extending out from central L1641N clearly point away from L1641N-124, this could be a shock along the wall of the cavity as the flow interacts with the surrounding molecular cloud. In the optical lines $\text{H}\alpha$ and [SII] (see Reipurth et al. 1998) this jet (HH 303) is displaced to the West (pointing at 14P). Also, while most proper motions South of L1641N-124 point away from this source, there are several shocks to the North that point away from L1641N-115/116. Combining IR and optical observations, Reipurth et al. (1998) suggests that the southern flow is red-shifted (since it is not seen in the optical) and the northern flow is blue-shifted and seem to stretch 6.3 pc away including HH 306–310 in the optical. At the far South (6.5 pc away) HH 61/62 are seen at the southern edge of the L1641N cloud (where the extinction is low) and could form a counter-lobe of about equal length. This scenario agrees well with the red and blue-shifted lobes seen in CO observations (Fukui et al. 1988). The flow is probably oriented close to the plane of the sky since its fastest shocks have projected velocities above 200 km s^{-1} as shown in our proper motion measurements.

4.3. Other shocks

In Fig.3 we have used red arrows to mark proper motions of isolated H_2 knots with unknown origins (shocks 14R, 14 V and 16D). This has been done for completeness of the survey and the names have to do with the fact that they are located close to the corresponding flows although not part of them. Object 14R however has a proper motions that suggests that it could originate from a source in the central region. The proper motions and locations of H_2 objects 14M₂ and M₃ suggests two possibilities. They could originate from a source in the central region, but the observations are also in agreement with a bi-polar outflow from L1641N-145 (which is also bright at $24\mu\text{m}$) that has 14M₁–M₃ on one side and the chain of shocks 14N₁–N₄ to the other side.

Even though the shocks 9A and B (HH 299) are located very close to the young star L1641N-61 (see Figures 3 and 2) this is most likely just a coincidence as the geometry suggests that they are not physically related. As no proper motions are seen for these two shocks at our present time span and resolution this can however not be confirmed.

5. Summary and conclusions

We have made detailed observations of the Herbig-Haro (HH) flows in L1641N by observing two overlapping deep fields in the near-IR $2.12\mu\text{m}$ shock line of H_2 . Using previous observations, taken 9 years before, we also calculate proper motions for all shocks with projected velocities faster than about 30 km s^{-1} . Two major bi-polar HH flows are seen and most HH objects are shown to be part of either the large-scale roughly North-South oriented flow from central L1641N or a previously unseen HH flow in eastern L1641N. By combining this velocity survey with new Spitzer $24\mu\text{m}$ observations we have also found the outflow source of the eastern flow and found a candidate outflow source for the giant central N-S flow that we detect for the first time in the near-IR (K_S band). Extending a line from the eastern outflow source along the proper motion vector of the eastern lobe we find that HH 301 and HH 302, almost 1 pc away, most likely are part of this flow. The outflow source of the eastern flow, L1641N-172, is found to be the currently brightest mid-IR source in L1641N and seem to have brightened a lot during the last 20 years. We make the first detection of this source in the near-IR (K_S) and also find a near-IR reflection nebula pointing at the source. This could be the illuminated walls of a cone-shaped cavity cleared out by the eastern lobe of the outflow. The tangential velocities of the central flow close to the outflow source has a explosion-like structure, with a fast moving bow shock followed by slower and slower moving shocks closer to the source. We find a bow shock in the northern and southern lobes that were ejected about 730 and 780 years ago respectively, probably belonging to the same outburst. There is another strong bow shock further out in the North flow that was ejected in a previous outburst about 2200 years ago.

Acknowledgements. The Swedish participation in this research is funded by the Swedish National Space Board. This publication made use of the NASA/IPAC Infrared Science Archive, which is operated by the Jet Propulsion Laboratory, California Institute of Technology, under contract with the National Aeronautics and Space Administration, and data products from the Two Micron All Sky Survey, which is a joint project of the University of Massachusetts and the Infrared Processing and Analysis Center/California Institute of Technology, funded by the National Aeronautics and Space Administration and the National Science Foundation. We would also like to thank Thomas Stanke for the $2.12\mu\text{m}$ H_2 mosaic we used for the first epoch of our proper motion calculations.

References

- Chen H., Tokunaga T., Strom K.M., Hodapp K.W., 1993, ApJ 407, 639
- Chen H., Ohashi N., Umemoto T., 1996, AJ 112, 717
- Coppin K.E.K., Davis C.J., Micono M., 1998, MNRAS, 301, L10
- Davis C.J., Eislöffel J., 1995, A&A 300, 851
- Fukui Y., Sugitani K., Takaba H., et al., 1986, ApJ 311, L85
- Fukui Y., Takaba H., Iwata T., et al. 1988, ApJ 325, L13
- Gålfalk M., Olofsson G., Kaas A.A., et al., 2004, A&A 420, 945
- Gålfalk M., 2005, NOT Annual report 2004, p18-19
- Gålfalk M., Olofsson G., 2007, A&A, to be submitted
- Harvey P.M., Chapman N., Lai S-P., et al., 2006, ApJ 644, 307
- Hodapp K.W., Deane J., 1993, ApJS 88, 119
- Kaufman M.J., Neufeld D.A., 1996, ApJ 456, 611
- Lee J.-K., Burton M.G., 2000, MNRAS, 315, 11
- Mader S.L., Zealey W.J., Parker Q.A. et al., 1999, MNRAS, 310, 331
- Micono M., Davis C.J., Ray T.P., et al., 1998, ApJ, 494, L227

Noriega-Crespo A., Morris P., Marleau F.R., et al., 2004, ApJS 154, 352
Raga A.C., 1993, Ap&SS, 208, 163
Reipurth B., Devine D., Bally J., 1998, AJ, 116, 1396
Sakamoto S., Hasegawa T., Hayashi M., et al, 1997, ApJ 481, 302
Smith M.D., 1994, MNRAS, 266, 238
Smith M.D., Khanzadyan T., Davis C.J., 2003, MNRAS, 339, 524
Smith M.D., Rosen A., 2005, MNRAS 357, 1370
Stanke T., McCaughrean M.J., Zinnecker H., 1998, A&A 332, 307
Stanke T., Williams J.P., 2006 / 2007, AJ, accepted
Strom K., Margulis M., Strom S., 1989, ApJ 346, L33